RSC Advances

COMMUNICATION

Unprecedented catalytic activity of Mn_3O_4 nanoparticles: potential lead of a sustainable therapeutic agent for hyperbilirubinemia†

Cite this: *RSC Adv.*, 2014, **4**, 5075

Received 3rd October 2013
Accepted 10th December 2013

DOI: 10.1039/c3ra45545a

www.rsc.org/advances

Anupam Giri,[a] Nirmal Goswami,[a] Chandan Sasmal,[b] Nabarun Polley,[a] Dipanwita Majumdar,[c] Sounik Sarkar,[d] Sambhu Nath Bandyopadhyay,[b] Achintya Singha[c] and Samir Kumar Pal*[a]

We report an unprecedented catalytic decomposition of aqueous bilirubin solution, without any photo-activation, by citrate functionalized Mn_3O_4 nanoparticles (NPs). *In vitro* reactivity of the catalyst on the whole blood specimen of hyperbilirubinemia patients revealed that the catalyst can significantly suppress the total bilirubin level in the blood specimens.

Bilirubin is a family of orange-yellow pigments produced from the breakdown of the heme group in the red blood cells.[1] An increased concentration of bilirubin in the blood (hyperbilirubinemia) leads to jaundice and is a potential cause of permanent brain damage or even death in newborn babies.[1a,2] Bilirubin accumulates in the blood and tissues of those suffering from liver diseases and also in case of diseases associated with increased red blood cell destruction (haemolytic anaemias), gives rise to severe hyperbilirubinemia and neurotoxicity.[3] Conventional treatment those are currently available for severe hyperbilirubinemia includes phototherapy,[4] haemoperfusion,[5] haemodialysis and exchange blood transfusion.[6] Phototherapy treatment involves mainly long exposure of blue light, 10–12 hours per day.[4] Although effective, phototherapy is cumbersome and inconvenient and its efficacy may diminish with age because of increased skin thickness and decreased surface/mass ratio.[7] Exchange transfusion or haemoperfusion is also associated with several known disadvantages such as significant morbidity, and even mortality.[8] Thus, to avert these harmful effects, a worthwhile challenge, therefore, is to develop facile less invasive alternative treatment strategies for direct removal of bilirubin from blood plasma of patients suffering from hyperbilirubinemia.

The development of new catalysts – be they homogeneous or heterogeneous, with novel reactivity and selectivity towards a desired chemical transformation having direct biological and medical significance, is highly desirable.[9] Mixed-valence oxides of transition metals with a spinel structure are an important class of metal oxides that have been investigated extensively as catalyst due to their efficient activity, low cost, simple preparation, and high stability. In particular, research on Mn_3O_4 has been a key topic because of their excellent bifunctional oxygen electrode activity,[10] photocatalytic activity[11] and potential applications in several redox reactions.[12]

Herein, we describe a convenient nanochemistry based approach for highly efficient catalytic decomposition of aqueous bilirubin solution by citrate functionalized Mn_3O_4 NPs (citrate–Mn_3O_4 NPs), in absence of any photo-activation. It is revealed that the mixed valence state of Mn (+2, +3 and +4) along with the functional groups on the surface coordinating ligands of Mn_3O_4 NPs lead to this exceptional catalytic activity. The *in vitro* studies of citrate–Mn_3O_4 NPs on the whole blood specimens of hyperbilirubimia patients show that, the NPs can selectively reduce the bilirubin level (both conjugated and unconjugated) in the blood specimens very fast and without any significant alteration of other essential blood parameters. Given the remarkable efficiency of the NPs towards the suppression of the blood bilirubin level combined with their colloidal stability and biocompatibility indicates the promise of this NPs in direct therapeutic applications against hyperbilirubinemia.

We have synthesized the bulk Mn_3O_4 NPs following a reported procedure[13] by Lei *et al.* As shown in Fig. S1 (in ESI†), all X-ray diffraction peaks of as-prepared Mn_3O_4 NPs is perfectly indexed in the literature to the tetragonal structure of Mn_3O_4 NPs. In the process to explore the catalytic potential of Mn_3O_4 NPs upon functionalization, we have focused on using the ligands having functional groups that favours the interaction between the ligand decorated NPs with the analyte of interest.

[a]*Department of Chemical, Biological and Macromolecular Sciences, S. N. Bose National Centre for Basic Sciences, Block JD, Sector III, Salt Lake, Kolkata 700 098, India. E-mail: skpal@bose.res.in*

[b]*Department of Obstetrics & Gynaecology, Institute of Post Graduate Medical Education and Research (IPGME&R), 244 A. J. C Bose Road, Kolkata, 700 020, India*

[c]*Department of Physics, Bose Institute, 93/1, Acharya Prafulla Chandra Road, Kolkata 700 009, India*

[d]*Department of Biochemistry, University of Calcutta, 35 Ballygunge Circular Road, Kolkata 700 019, India*

† Electronic supplementary information (ESI) available: See DOI: 10.1039/c3ra45545a

Bilirubin (BR) consists of an open chain of four pyrrole-like rings (tetrapyrrole). So, to ensure efficient interaction we have functionalized the as-prepared Mn_3O_4 NPs employing a carboxylate-rich biocompatible ligand, tri-sodium citrate. TEM study has been carried out in order to characterize the water soluble citrate–Mn_3O_4 NPs in details. As shown in Fig. 1a, citrate–Mn_3O_4 NPs are nearly spherical in shape with an average diameter of 3.63 ± 0.28 nm (Fig. 1c). The HRTEM image (Fig. 1b) confirms the crystalline nature of the citrate–Mn_3O_4 NPs having interplanar distance of 0.310 nm, corresponding to the (112) plane of the crystal lattice. Fig. 1d illustrates the UV-vis absorption spectrum of citrate–Mn_3O_4 NPs and citrate, at pH ~7. The observed peak at around 290 nm (in the inset) could be assigned to the possible high energy ligand-to-metal charge transfer transition (LMCT) involving citrate–Mn^{4+} interaction. The other bands at 430, 565 and 752 nm are attributed to the Jahn–Teller (J–T) distorted d–d transitions centered over Mn^{3+} ions in citrate–Mn_3O_4 NPs.[14]

To determine the catalytic performance of citrate–Mn_3O_4 NPs in BR decomposition at pH = 7.4 and without any photo-activation, the characteristic absorbance of BR at 450 nm has been chosen for monitoring the kinetic study using UV-vis spectroscopy. Fig. 2 shows the relative concentration (C_t/C_0) of BR plotted against reaction time. As shown in the figure, in absence of catalyst, only a slight decomposition (less than 3%) of BR can be observed after 50 min, whereas about 92% of BR is decomposed in the presence of citrate–Mn_3O_4 NPs and a concomitant colour change of BR from bright yellow to colourless was observed (Fig. S2 in ESI†). Therefore, the observed colour change is attributed to catalytic decomposition of BR and the decomposition curve has been found to follow a first-order exponential equation with kinetic rate constant (k) of 6.62 × 10^{-2} min^{-1}. Time dependent Raman study of aqueous solution of BR (Fig. S3 in ESI†) also reveals significant perturbations of its main characteristic bands for lactam and pyrrole moieties lie within 1100–1700 cm^{-1},[15] upon addition of catalyst into the solution. To ensure that the catalyst could be recycled without any significant loss of activity, we have tested the recyclability of the catalyst up to 20 cycles (inset of Fig. 2 and S4 in ESI†). Through comparing the morphology of the fresh and used citrate–Mn_3O_4 NPs catalyst (Fig. S5†) it is found that there is no obvious change in the morphology before and after the catalytic process, which is in line with its repeated catalytic activity.

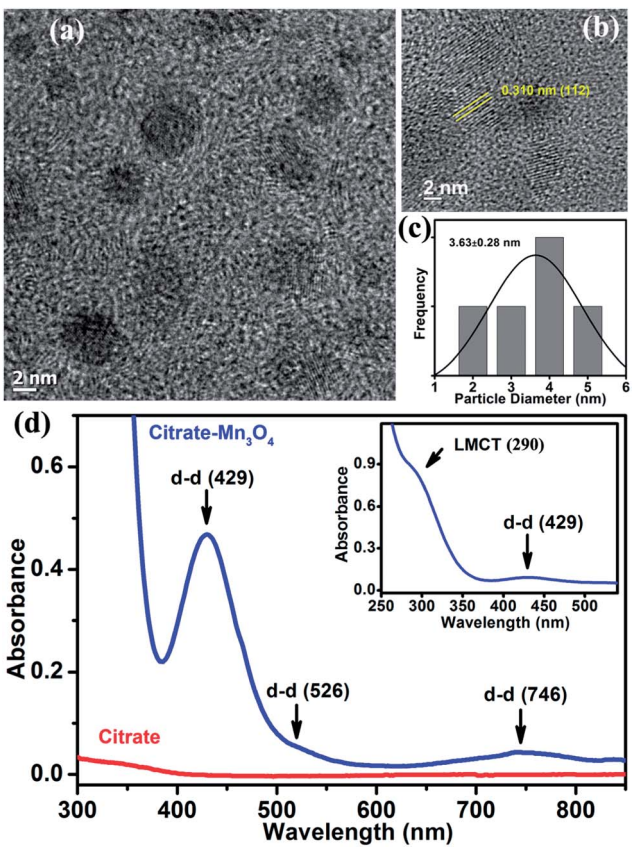

Fig. 1 (a) TEM image of citrate–Mn_3O_4 NPs. (b) Lattice fringes in the corresponding HRTEM image indicating high crystalline nature of the NPs. (c) Size distribution of citrate–Mn_3O_4 NPs. (d) UV-vis absorption spectrum for citrate–Mn_3O_4 NPs and citrate at pH ~7. Inset shows higher energy strong absorption band due to LMCT for very dilute citrate–Mn_3O_4 NPs solution.

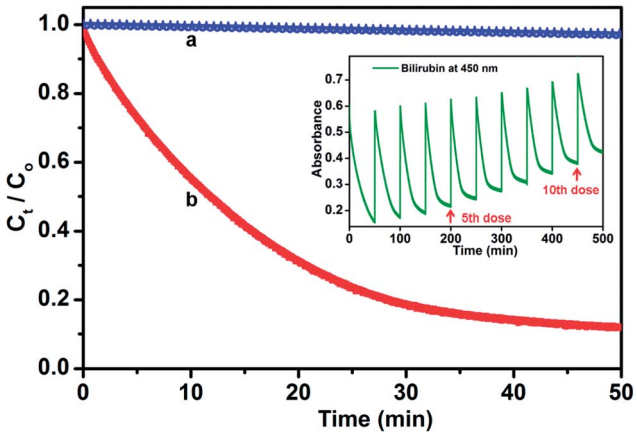

Fig. 2 Catalytic decomposition of the aqueous solution of bilirubin in absence of any photo activation. Relative concentration (C_t/C_0) *versus* time plots for the catalytic decomposition of bilirubin (UV-vis absorbance of bilirubin monitored at 450 nm) in the absence (a) and presence (b) of citrate–Mn_3O_4 NPs are shown. Inset shows the cycling curves of bilirubin decomposition kinetics upto 10 cycles.

To elucidate the nature of the catalytic decomposition products, we have phase transferred the products from aqueous to chloroform medium, in order to avoid possible interference of the catalyst in the characterization process and also considering solubility of previously reported BR degradation products in less polar solvents.[16] Fig. 3a shows the UV-vis absorption spectrum of the decomposition products in chloroform and the inset represents photoluminescence spectra (λ_{ex} = 350 nm) of the same. UV-vis absorption bands at 248 and 312 nm along with the ~450 nm photoluminescence peaks are closely resembled with previously reported photo-oxidation product of BR, methylvinylmaleimide (MVM).[16] The identity of the 278 nm absorption band is not known at this time, which could possibly be due to the formation of other decomposition products. To investigate the mechanistic insight of the catalytic process and the active sites of the nanoparticles involved, we have

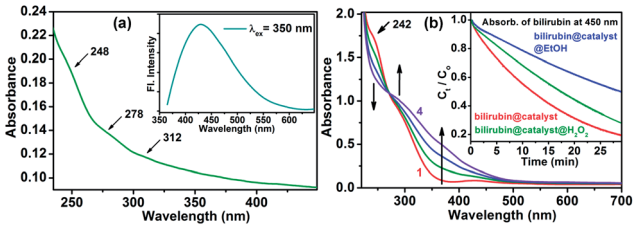

Fig. 3 (a) UV-vis absorption spectrum of bilirubin decomposition products in chloroform. Inset represents the photoluminescence spectra (λ_{ex} = 350 nm) of the products at room temperature. (b) Illustrates the UV-vis absorption spectra of 10 μM aqueous solution of citrate–Mn_3O_4 NPs after complete decomposition (takes 2 h) of each dose of bilirubin into the solution at pH = 7.4. Inset shows the plots of relative concentration (C_t/C_0) *versus* time for bilirubin decomposition (monitored at 450 nm) in presence of citrate–Mn_3O_4 NPs, citrate–Mn_3O_4@H_2O_2 and citrate–Mn_3O_4@EtOH.

monitored the changes in the characteristic ligand to metal charge transfer bands (LMCT, which are originated due to the interaction of $Mn^{3+/4+}$ centres in the NPs with the surface bound citrate ligands) of citrate–Mn_3O_4 NPs employing UV-vis spectroscopy, upon stepwise addition of BR. Fig. 3b illustrates the UV-vis absorption spectra of 10 μM aqueous solution of citrate–Mn_3O_4 NPs (catalyst) after complete decomposition (takes 2 h) of each dose of BR into the solution at pH = 7.4. The characteristic absorption bands of the catalyst at 242 and 288 nm are attributed to the LMCT bands originated due to Mn^{3+}–citrate and Mn^{4+}–citrate interactions, respectively.[14b,17] The stepwise addition of BR to the aqueous solution of catalyst resulted in a monotonous decrease of absorption at 242 nm and subsequent increase in absorption at 288 and 368 nm, accompanied by the formation of an isosbestic point at 270 nm (Fig. 3b). The decrease of absorption at 242 nm could be due to the possibility that, upon stepwise addition of BR, more and more Mn^{3+} ions at the NPs surface are converted to Mn^{4+} state and the growing amount of Mn^{4+}–citrate charge transfer states has been witnessed by the increase in absorption at 288 and 368 nm.[14b] The appearance of an isosbestic point at 270 nm is evidence for two absorbing systems namely the Mn^{3+}–citrate LMCT band at 242 nm and Mn^{4+}–citrate LMCT bands at 288 and 368 nm. The definite proof of the involvement of Mn^{3+} and its conversion into Mn^{4+} state during the catalytic process was obtained from pH dependent study. We have evaluated the catalytic efficiency of citrate–Mn_3O_4 NPs at pH-7 and pH-10. As shown in Fig. S6,† at pH-10, catalytic efficiency of the NPs reduced very significantly. This phenomenon is consistent with the fact that, in acidic/neutral pH, Mn^{3+} ions are unstable and tend to disproportionate into Mn^{2+} and Mn^{4+}, whereas it is stabilized by the comproportionation of Mn^{2+} and Mn^{4+} in alkaline conditions.[18] Thus, due to its stability, Mn^{3+} in the NPs surface dose not tends to react with BR at higher pH. Given the valence state conversion of Mn from +3 to +4 states upon increasing dose of BR, we anticipated that the catalytic outcome would be the reductive decomposition products of BR. However, as discussed earlier we have found that, spectroscopic signature of the resulting compound closely resemble with the oxidative decomposition product (MVM) of BR. Thus the catalytic process followed a different pathway other than a direct redox reaction involving $Mn^{3+/4+}$ metal ions at the NPs surface and BR molecules. To investigate whether the catalytic process is associated with any

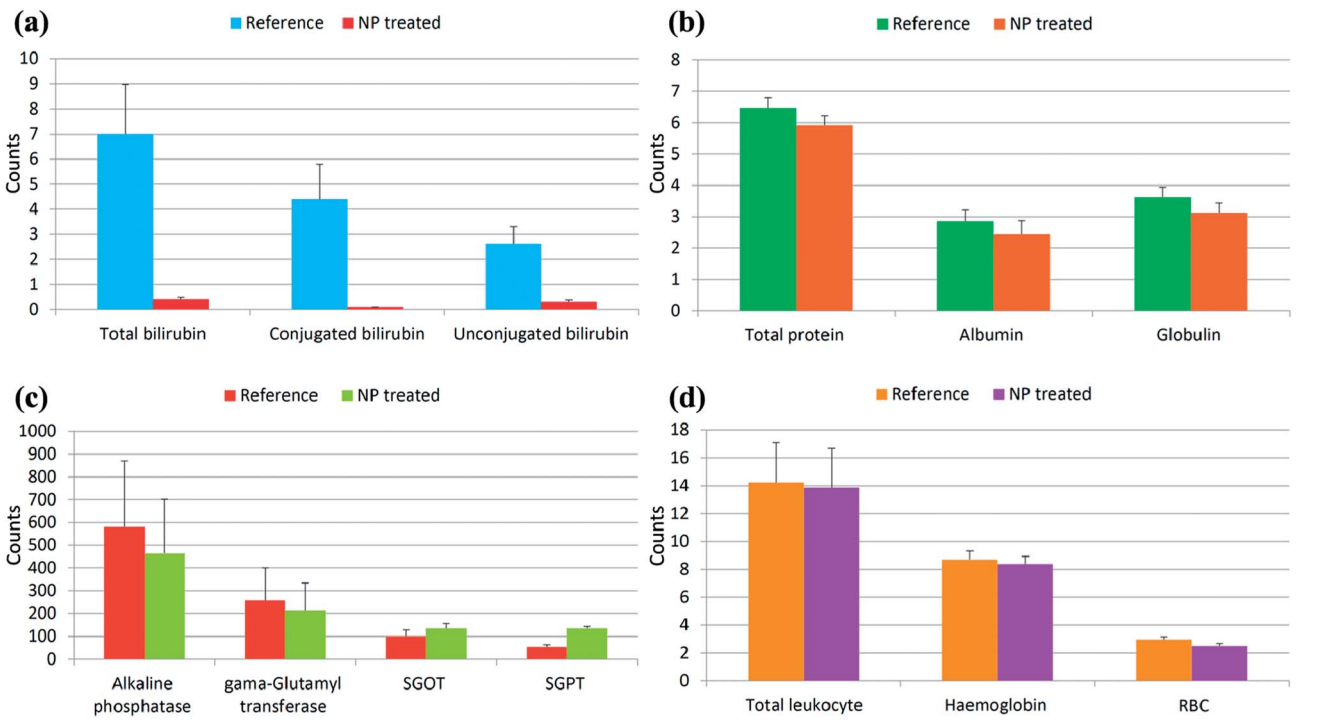

Fig. 4 Assay results of different parameters in the blood specimens, with and without treatment (reference) with citrate–Mn_3O_4 NPs. Data are plotted as mean + standard error of the mean (SEM) [n = 12].

radical pathways, we have performed the BR decomposition study (as shown in Fig. 2) in presence of a radical initiator (H_2O_2, a source of $^{\bullet}OH$ radical) and a radical scavenger (ethanol) separately. As shown in the inset of Fig. 3b, in both cases, a slower catalytic rates have been observed, which validates the role of $^{\bullet}OH$ radicals in the catalytic process. Although, slower rate in case of H_2O_2 seems unexpected, however, this result can be explained by the fact that, H_2O_2 itself can influence the conversion of Mn^{+3} to Mn^{+4} states to a great extent and consequently diminish the number of active catalytic sites on the NPs surface. Therefore, we hypothesized that, the origin of such unprecedented catalytic activity might be initiated by the conversion of Mn^{3+} to Mn^{+4} states at the NPs surface and subsequent formation of reactive oxygen species[19] (such as $^{\bullet}OH$ radicals), that ultimately leads to the decomposition of the analyte, BR.

Having developed the highly active citrate–Mn_3O_4 NPs for BR decomposition, we sought to test their *in vitro* effectiveness by adding the catalyst to human peripheral blood specimens collected from hyperbilirubinemia patients. Our primary objective was to evaluate the BR levels of the blood specimens with and without treatment by citrate–Mn_3O_4 NPs. Fig. 4 represents the assay results, performed over blood specimens of hyperbilirubinemia patients. As shown in Fig. 4a, average BR level (total, conjugated and unconjugated) in the blood specimens of 12 patients, treated with citrate–Mn_3O_4 NPs, reduced down remarkably with respect to the reference (Table 1). It has also been observed that conjugated portion of the total BR decreases more than its unconjugated counterpart, this is expected, as the water soluble glucuronic acid conjugated portion get higher chance to interact with NPs than the albumin bound unconjugated part. This observation is further supported by our initial findings that catalytic decomposition of HSA bonded BR is slower compared to free BR (Fig. S7 in ESI†). In the same blood specimens where we have evaluated BR level, simultaneously, we have also checked the effects of citrate–Mn_3O_4 NPs on other liver function parameters such as total protein, albumin, globulin, alkaline phosphatase, γ-glutamyl transferase, SGOT and SGPT. As shown in Fig. 4b and c, the change in the parameters upon interaction with citrate–Mn_3O_4 NPs is statistically insignificant (Table S1,† *P* value >0.05), except in case of SGPT. Exact reason for the increase of SGPT upon interaction with the NPs is not known in the present time and needs further investigation. In case of different haematological parameters such as haemoglobin, red blood cell (RBC) count and total leukocyte count (Fig. 4d and Table 2), it has been found that there is also insignificant variation (*P* value >0.05) upon treatment of the blood specimens with citrate–Mn_3O_4 NPs. Nominal variation in the count of RBC and total leukocyte cells in the NP treated specimens, directly indicates the blood biocompatibility of citrate–Mn_3O_4 NPs. Moreover, we have also evaluated the effectiveness of citrate–Mn_3O_4 NPs against the conventional blue light used in phototherapy, towards BR decomposition. As shown in Fig. S8b in ESI,† citrate–Mn_3O_4 NPs exhibit comparable efficiency against blue light along with an added advantage of dark reactivity.

Table 1 *In vitro* effect of citrate–Mn_3O_4 NPs on the bilirubin level of blood specimen. Data are expressed as mean ± standard deviation [$n = 12$]. *P* values indicating statistical significance, were determined by Student's unpaired *t*-test. *P* values less than 0.05 considered statistically significant

Parameters (mg dL^{-1})	Reference specimen	NP treated specimen	*P* value
Total bilirubin	7.01 ± 6.80	0.42 ± 0.29	<0.0001
Conjugated bilirubin	4.40 ± 4.81	0.10 ± 0	<0.0001
Unconjugated bilirubin	2.62 ± 2.36	0.32 ± 0.29	0.0001

Table 2 *In vitro* effect of citrate–Mn_3O_4 NPs on haemoglobin and different blood cells. Data are expressed as mean ± standard deviation [$n = 12$]. *P* values were determined by Student's unpaired *t*-test

Parameters	Reference specimen	NP treated specimen	*P* value
Haemoglobin (gm dL^{-1})	8.70 ± 1.93	8.36 ± 1.85	0.70
RBC count ($\times 10^6/\mu L$)	2.97 ± 0.64	2.50 ± 0.67	0.13
Total leukocyte count ($\times 10^9/L$)	14.23 ± 9.01	13.86 ± 8.83	0.92

In summary, we have for the first time demonstrated that highly water-soluble citrate–Mn_3O_4 NPs can catalytically decompose yellow aqueous solution of bilirubin to its colourless oxidative break down products in a very quick time and most importantly, without any photo-activation. Mechanistic studies on the catalytic process have resulted in greater understanding of the catalytic cycle and additional insight into the active sites of the nanoparticles involved. Furthermore, the remarkable *in vitro* reactivity of the catalyst towards the suppression of bilirubin level in the whole blood specimens of hyperbilirubinemia patients, without much affecting other important blood constituents, represents a great promise of citrate–Mn_3O_4 NPs in direct therapeutic applications against hyperbilirubinemia.

The authors would like to thank Prof. Anjan Kr. Dasgupta at Department of Biochemistry, University of Calcutta and Prof. Avijit Hazra of IPGME&R, Kolkata, for insightful discussions. A. G. thanks UGC, India, for fellowship. N. G. thanks CSIR, India, for fellowship. We thank Department of Science and Technology (DST), Government of India, for financial grants DST/TM/SERI/2k11/103 and SB/S1/PC-011/2013.

Notes and references

1 (*a*) J. Kapitulnik, *Mol. Pharmacol.*, 2004, **66**, 773–779; (*b*) J. Fevery, *Liver Int.*, 2008, **28**, 592–605.
2 R. Brodersen, *J. Biol. Chem.*, 1979, **254**, 2364–2369.
3 X. Wang, J. R. Chowdhury and N. R. Chowdhury, *Curr. Paediatr.*, 2006, **16**, 70–74.
4 C. N. Van Der Veere, M. Sinaasappel, A. F. McDonagh, P. Rosenthal, P. Labrune, M. Odiévre, J. Fevery, J. Otte, P. McClean, G. Bürk, V. Masakowski, W. Sperl,

A. P. Mowat, G. M. Vergani, K. Heller, J. P. Wilson, R. Shepherd and P. L. Jansen, *Hepatology*, 1996, **24**, 311–315.
5 S. Sideman, L. Mor, M. Mihich, S. Lupovich, J. M. Brandes and M. Zetzer, *Contrib. Nephrol.*, 1982, **29**, 90–100.
6 (*a*) S. Murki and P. Kumar, *Semin. Perinatol.*, 2011, **35**, 175–184; (*b*) B. Xia, G. Zhang and F. Zhang, *J. Membr. Sci.*, 2003, **226**, 9–20.
7 G. Toietta, V. P. Mane, W. S. Norona, M. J. Finegold, P. Ng, A. F. McDonagh, A. L. Beaudet and B. Lee, *Proc. Natl. Acad. Sci. U. S. A.*, 2005, **102**, 3930–3935.
8 W. J. Keenan, K. K. Novak, J. M. Sutherland, D. A. Bryla and K. L. Fetterly, *Pediatrics*, 1985, **75**, 417–441.
9 (*a*) G.-E. Wang, G. Xu, M.-S. Wang, J. Sun, Z.-N. Xu, G.-C. Guo and J.-S. Huang, *J. Mater. Chem.*, 2012, **22**, 16742–16744; (*b*) S.-Y. Peng, Z.-N. Xu, Q.-S. Chen, Y.-M. Chen, J. Sun, Z.-Q. Wang, M.-S. Wang and G.-C. Guo, *Chem. Commun.*, 2013, **49**, 5718–5720.
10 Y. Gorlin and T. F. Jaramillo, *J. Am. Chem. Soc.*, 2010, **132**, 13612–13614.
11 Y. Li, H. Tan, X.-Y. Yang, B. Goris, J. Verbeeck, S. Bals, P. Colson, R. Cloots, G. Van Tendeloo and B.-L. Su, *Small*, 2011, **7**, 475–483.
12 (*a*) E. R. Stobbe, B. A. de Boer and J. W. Geus, *Catal. Today*, 1999, **47**, 161–167; (*b*) R. Alizadeh, E. Jamshidi and G. Zhang, *J. Nat. Gas Chem.*, 2009, **18**, 124–130.
13 S. Lei, K. Tang, Z. Fang and H. Zheng, *Cryst. Growth Des.*, 2006, **6**, 1757–1760.
14 (*a*) A. Giri, N. Goswami, M. Pal, M. T. Zar Myint, S. Al-Harthi, A. Singha, B. Ghosh, J. Dutta and S. K. Pal, *J. Mater. Chem. C*, 2013, **1**, 1885–1895; (*b*) M. E. Bodini, L. A. Willis, T. L. Riechel and D. T. Sawyer, *Inorg. Chem.*, 1976, **15**, 1538–1543.
15 B. Yang, M. D. Morris, M. Xie and D. A. Lightner, *Biochemistry*, 1991, **30**, 688–694.
16 W. E. Kurtin, *Photochem. Photobiol.*, 1978, **27**, 503–509.
17 A. Giri, N. Goswami, M. S. Bootharaju, P. L. Xavier, R. John, N. T. K. Thanh, T. Pradeep, B. Ghosh, A. K. Raychaudhuri and S. K. Pal, *J. Phys. Chem. C*, 2012, **116**, 25623–25629.
18 T. Takashima, K. Hashimoto and R. Nakamura, *J. Am. Chem. Soc.*, 2011, **134**, 1519–1527.
19 M. Purdey, *Med. Hypotheses*, 2000, **54**, 278–306.